# Reconstructing Surface Eruptive Sequence of 2018 Small Phreatic Eruption of Iwo-Yama Volcano, Kirishima Volcanic Complex, Japan by Infrasound Cross-correlation Analysis

**Dan Muramatsu** ( muramatsu@sevo.kyushu-u.ac.jp )
Kyushu University https://orcid.org/0000-0001-6968-770X
**Takeshi Matsushima**
Institute of Seismology and Volcanology, Faculty of Science, Kyushu University, Shimabara, Japan
**Mie Ichihara**
Earthquake Research Institute, The University of Tokyo, Tokyo, Japan

**Express Letter**

**Keywords:** Volcano infrasound, Phreatic eruption, Multiple-vent activities, Cross-correlation analysis, Iwo-yama volcano, Monitoring

**Posted Date:** November 6th, 2020

**DOI:** https://doi.org/10.21203/rs.3.rs-102486/v1



**Version of Record:** A version of this preprint was published on January 5th, 2021. See the published version at https://doi.org/10.1186/s40623-020-01344-6.

# Abstract

The Iwo-yama volcano of the Kirishima Volcanic Complex in Japan had a small phreatic eruption in April 2018, which formed multiple vents. The activity was recorded by two infrasound sensors and two monitoring cameras which had been installed within 1 km of the vents. This study identified infrasonic signals from the multiple vents by a cross-correlation analysis between the two infrasound sensors. The analysis successfully revealed the signals from two main eruption craters and constrained the infrasound onsets at the individual vents in the two craters. We combined the results with the images from the cameras and reconstructed the sequence of the small phreatic eruption of Iwo-yama. Notably, the intense eruption accompanying remarkable infrasound delayed several hours to the eruption onset at each of the two craters. This study provides a sequence of the activities of the multiple vents in a phreatic eruption, which will be useful for understanding the phreatic eruption mechanism and hazard assessments.


# Introduction

Diverse volcanic activities produce acoustic waves below 20 Hz called infrasound, which are inaudible to humans. Infrasound observation is a widely used technique to capture surface phenomena associated with various volcanic activities (i.e., Fee and Matoza 2013). Some examples are targeting the Strombolian eruption (Vergniolle and Brandeis 1996; Delle Donne and Ripepe 2012; Ishii et al. 2019), Vulcanian eruption (Yokoo et al. 2009; Anderson et al. 2018), Subplinian–Plinian eruption (Matoza et al. 2009; Fee et al. 2010), Hawaiian eruption and lava lake activity (Garcés et al. 2003; Bouche et al. 2010), eruption columns (Yamada et al. 2017, 2018; Perttu et al. 2020), and pyroclastic flow (Yamasato 1997; Ripepe et al. 2010). An effective and commonly used method to investigate the infrasonic source location is an array observation composed of more than three sensors. This enables signal beamforming for the discrimination of different activities at multiple vents and distinguishing them from uncorrelated local noise or non-volcanic infrasonic sources (Ripepe and Marchetti 2002; Johnson and Ripepe 2011; Yamakawa et al. 2018; Matoza et al. 2019). However, the construction and maintenance of arrays in volcanic regions is not easy, and only a few volcanoes are equipped with permanent infrasonic arrays. Although infrasound detection methods using a single infrasound microphone and a collocated seismometer have been proposed (Ichihara et al. 2012; McKee et al. 2018), they are not applicable when a volcano is seismically very active. Alternatively, using a pair of microphones significantly improves infrasound detection (Castaño et al. 2020) and helps to estimate source locations (Walsh et al. 2019).

In phreatic eruptions, multiple vents are frequently formed one after another at the ground surface (e.g., Yukutake et al. 2017). Identifying multiple vent activities is essential for understanding the transition process of phreatic eruptions and hazard assessments. The 2018 eruption of the Iwo-yama volcano of the Kirishima Volcanic Complex (KVC) in Japan is a case of phreatic eruptions with successive vent formations. Two infrasonic sensors and monitoring cameras recorded the events within 1 km of the vents. In this study, we used an acoustic cross-correlation analysis between the two infrasound sensors to reveal the activities of the individual vents. We also referred to the monitoring images and then, reconstructed the sequence of the small phreatic eruption at the Iwo-yama volcano.

## Data

# Infrasonic data

Infrasonic data were collected at KU.EBQ7 station, 387 m southwest of the summit of Iwo-yama, and KU.KREB station, 842 m west of the summit (Fig. 1a). Infrasound was recorded using a Hakusan SI104 microphone (Hakusan Corporation, Japan) at KU.EBQ7 (hereafter referred to as MC1) at 200-Hz sampling frequency and a Hakusan SI102 microphone at KU.KREB (MC2) at 100 Hz. Both microphones have flat responses in a frequency range above 0.05 Hz. All the time-series data were logged continuously by 24-bit digitizers.

# Monitoring camera

Monitoring camera data were provided by the Kagoshima Local Meteorological Office of the Japan Meteorological Agency (JMA). There were two video cameras around Iwo-yama volcano. The Iwo-Yama-Minami monitoring camera (CAM1), was located 204 m to the south of the summit and the Ebinokogen monitoring camera (CAM2), was located 930 m to the west (Fig. 1a). Because these are visible light cameras, volcanic activity during night could not be captured. The sampling rate was approximately 6 s. The vents formed in front of either one of the cameras, and therefore, their activities were successfully captured during the daytime.

# Overview of the 2018 small phreatic eruption of Iwo-yama

KVC is composed of ~ 20 volcanoes and is located in the southern part of Kyushu Island, Japan (Fig. 1a). Iwo-yama is one of the active cones of KVC, holding subsurface hydrothermal systems and surface geothermal activities (Tsukamoto et al. 2018). From April 19–21, 2018, a small phreatic eruption occurred at Iwo-yama and emitted an ash-steam mixture up to 500 m from the vents. During this eruption, infrasonic signals were recorded by the observation sites near the vents (Fig. 1a). The eruptive activity was localized in two areas, which were the Iwo-yama South Craters (hereinafter, South Crater), consisting of several sub-craters, and Iwo-yama West Crater (hereinafter, West Crater) (Tajima et al. 2020). The craters were composed of several vents, namely S1 to S7 in South Crater and W1 to W7 in West Crater (Fig. 1b). The eruption began at vents S1 and S5 in South Crater from 15:39 on April 19, 2018, and the other vents were subsequently formed and merged into three sub-craters (Tajima et al. 2019). These were vents S1–S3 to the crater Y3, S4–S6 to the crater Y2a, and S7 to the crater Y2b (Fig. 1b). Hereafter, we refer to these three sub-craters (Y2a, Y2b, and Y3) as vents because our analysis does not have resolution to discriminate individual vents (S1–S7) in South Crater. At approximately 16:30 on April 20, steaming began 500 m to the west of South Crater, and the vents (W1–W7) formed before the morning of April 21. The vents W3 and W4 grew to a crater, around which ashy deposits and ejecta were observed. It is considered that the ejection occurred in the evening of April 20 (Tajima et al. 2020). However, the eruption time in the West Crater area was not logged by the video recordings as it was nighttime. After the eruption, vigorous fumarolic activity and hot water swelling from the vents continued for over a year.

Figure 2 shows the waveform and spectrogram of the infrasound recorded by MC2, and the snapshots taken by the monitoring cameras that captured surface phenomena at the two crater areas. During the entire period from 15:00 on April 19 to 7:00 on April 21 (Figs. 2a and 2b), tremor-like infrasound, with an amplitude of up to ~ 1 Pa consisting of two frequency bands, 1–7 Hz and 7–20 Hz, was observed. The eruption onset in South Crater was clearly captured by CAM1 (Figs. 2c and 2d) and was recognized by the sudden increase in the infrasound amplitude (Figs. 2a and 2b). The West Crater area was recorded by CAM2, where faint fumaroles began rising at approximately 16:30 on April 20 (Figs. 2e and 2f). However, the time of the small eruption from vents W3 and W4 could not be confirmed with the monitoring camera recordings. We aim to distinguish the acoustic signals of West Crater from those of South Crater.

## Method

# Cross-correlation analysis

We conducted an acoustic cross-correlation analysis between two microphones, MC1 (KU.EBQ7) and MC2 (KU.KREB); the distance between MC1 and MC2 is 585 m. Walsh et al. (2019) used a similar method for analyzing the phreatic eruption of White Island, New Zealand. They showed that the lag time of infrasound obtained by a cross-correlation analysis was consistent with the eruption vent locations inferred from the seismic tremor amplitude distribution and concluded that the eruption signals originated from a single vent. In this study, we attempted to distinguish and constrain the activity of multiple vents.

We investigated the temporal change of the cross-correlation coefficient

$$R(t,\tau) = R[\tau; P_1(t,x_1), P_2(t,x_2)],$$

where P1 and P2 are the acoustic signals recorded at points x1 and x2, respectively, and τ is the lag time of P1 to P2. We calculated R(t,τ)using time windows of a fixed length of 5 s starting at t and sliding with 60% overlaps. The result is graphically displayed on the t-τ axis. The function R(t,τ) has a peak at a particular lag time that corresponds to the acoustic travel time difference between the two observation points when a coherent acoustic signal exists. Depending on the signal's lag time and spectral features, the t-τ plot has a characteristic pattern that helps in identifying the signal. We separately performed correlation analyses in two frequency bands, 1–7 and 7–20 Hz, referring to the spectrogram (Fig. 2b).

# Estimation of expected lag time

Herein, the candidate source locations (South Crater and West Crater) are known, and therefore, the expected lag times are estimated. For simplicity, we assumed linear and isotropic propagation for acoustic waves. The expected lag time was then calculated as (d1-d2)/C, where d1 and d2 are the travel

distances of the signal from the source to the observation points x1 and x2, respectively, and c is the atmospheric sound speed. The atmospheric sound speed is calculated by assuming an ideal gas,

$$c = \sqrt{\gamma R_g T},$$

where γ is the heat capacity ratio (1.4), $R_g$ is the gas constant of air (287 J/kg/K), and T is the atmospheric temperature in K (Johnson 2003). The atmospheric temperature fluctuates with time. The wind speed and direction also affect the sound propagation velocity c. Although there was not a meteorological station present around Iwo-yama, the low-frequency noise level in the infrasound data suggested that the wind was weak. Therefore, we ignored the wind effect and calculated the theoretical temperature at an altitude of 1300 m from hourly temperature data collected at the Kakuto station (228 m a.s.l.) of JMA, which is the closest meteorological observation site. The estimated atmospheric temperature ranged from 272–296 K, and the resultant sound speed ranged from 330.7–345.0 m/s during the period from 15:00 on April 19 to 7:00 on April 21. Using these values, we estimated the possible ranges of the expected lag times. Assuming the source at South Crater (Y2a, Y2b, and Y3), the expected lag times are 1.46–1.57 s. If the source is located at West Crater (W3 and W4), the expected lag time is 0.70–0.74 s. The values for all the vents and craters are shown in Table A1 of Additional File 1.

# Results And Discussion

Figure 3 shows the results of the cross-correlation analysis. The top panel (Fig. 3a) shows the waveforms filtered at 1–7 Hz and 7–20 Hz. The middle and bottom panels show t-τ plots of the cross-correlation coefficient in the frequency ranges of 1–7 Hz (Fig. 3b) and 7–20 Hz (Fig. 3c), both of which exhibit high correlation values around τ =1.5 s after 15:39:45 on April 19. This lag time is equivalent to that expected for infrasound from South Crater, which confirms that its eruptive activity continued over the analyzed period after the onset. The correlation values in the lower-frequency band increase at 19:19:40 (Fig. 3b), similar to the amplitude values (Fig. 3a). Simultaneously, CAM1 captured the widening of the Y2a vent, which began at 18:40:51, with increased ash plumes from the vent (Additional File 2: Fig. A1). We consider that an intense eruption, accompanying remarkable low-frequency infrasonic signals, began at 19:19:40 after the vent widening. From around 3:57 on April 20, the correlation values around τ =1.5 s in the higher-frequency band intensified again (Fig. 3c). Besides, subtle peaks in τ <0.9 s, indicating West Crater signals, appear around 21:00 on April 20 in the 7–20 Hz band; however, the correlation pattern is unclear to constrain the onset (Fig. 3c).

We improved the resolution using the following procedure: The data were resampled up to 500 Hz by linear interpolation to increase the lag time resolution. We then calculated the cross-correlation coefficients for 5 s-long time windows sliding in 2 s, and progressively stacked them every 20 s. The results for the higher-frequency band are shown in Fig. 4, and the results for the lower-frequency band are provided in Additional File 3.

By analyzing the South Crater signals, the lag time of the initial stage of the eruption is 1.55 s, whereas that after the reincrease (3:57 on April 20) is 1.50 s. (Fig. 4b). Referring to the expected lag times of the South Crater signals (Table A1), we consider that the shortening of the correlation peak lag time by 0.05 s indicates the source shift from Y2a to Y3. The lag time starts shortening simultaneously with the vent widening at 18:40:51, and before the low-frequency power increase at 19:19:40 (Fig. 3b). The images from CAM1 also show increased ash plumes from Y3 with the widening of Y2a (Fig. A1). We interpret that Y3 was activated with the vent widening and then, from around 3:57 on April 20, became the main source of the higher-frequency infrasonic signals.

At West Crater, there is no clear correlation in the corresponding range $\tau$ before 21:00 (Fig. 4c), although CAM2 recorded faint steam clouds from around 16:30. A possible reason is that the signal was below the detection level, or was buried in the strong signal from South Crater. At 21:05:20 ± 10 s, a correlation peak appears around $\tau$ =0.83 s (Fig. 4c), which corresponds to vent W6 (Additional File 1: Table A1). The correlation decays after 22:00. Another peak then appears around $\tau$ =0.72 s from 21:42:20 ± 10 s (Fig. 4c), which we infer as the onset of the small eruption from vents W3 and W4 that erupted ash and ejecta.

The relationships between the correlation peak time lags and the source positions are subject to uncertainties regarding the atmospheric temperature and the local wind speed. We checked the validity of the interpretations described above. For South Crater, the peak at $\tau$ =1.55 s is related to Y2a with the atmospheric sound speed and temperature of 336 m/s and 281 K, respectively. If the signal is from Y3, the atmosphere should have 326 m/s and 265 K, respectively. Alternatively, if the peak at $\tau$ =1.50 s is made by Y2a, it requires 347 m/s and 300 K. These values are outside the range of the estimated atmospheric temperature. It is also unrealistic that the temperature increased by nearly 20 K from 4 pm to 4 am; neither can we assume that the wind speed increased more than 10 m/s when considering the low-frequency noise level of the infrasound data (Fig. 3a). For West Crater, if the peak at $\tau$ =0.83 s corresponds to W3 and W4 instead of W6, the sound speed and the atmospheric temperature need to be as low as 292 m/s and 212 K, respectively. If the peak at $\tau$ =0.72 s is vent W6, it requires extremely large values of 390 m/s and 379 K. Neither the wind can generate such propagation speeds.

We reconstructed the sequence of the multiple-vent activities of the 2018 small phreatic eruption of Iwo-yama (Fig. 5). South Crater began an eruption at 15:39 on April 19, mainly from Y2a (and Y2b). The vent widened from 18:40 to 19:19, following which the eruption intensified, accompanying lower-frequency infrasonic signals. Vent Y3 was activated with the Y2a widening and became the main source of higher-frequency infrasonic signals from 3:57 on April 20. The steam-emitting vents appeared in the West Crater area around 16:30 on April 20, and the eruptions accompanying infrasonic signals occurred from 21:05 successively, in multiple vents. These observations suggest that the intense eruptions with remarkable infrasonic signals started with several hours of delay after the onset of steaming or the appearance of the vents.

Several hours of delay in the vent formation accompanying ash falls with intensified seismic tremor after the infrasound onset was also observed in the 2015 small phreatic eruption of the Hakone volcano, Japan (Yukutake et al. 2017). The delay has been interpreted as the time for the hydrothermal fluid to reach the ground surface from a subsurface open-crack source, while the infrasound began concurrently with the crack opening by strain transfer (Yukutake et al. 2018). The time delay between the onset of surface phenomena and the intense eruptions can be a common feature of small-scale phreatic eruptions. Our results add another case and will be useful for considering the mechanism of the transition process of small-scale phreatic eruptions and assessing the hazards of eruptions that form multiple vents.

We found two types of signals in the frequency range and their temporal fluctuations and interpret this as the reflection of the dynamics and transition of the eruptive activity. At the West Crater area, the geological survey found ash deposits and fragments around W3 and W4 (Tajima et al. 2020), but only traces of mud flows from W6 (Tajima et al. 2019). Conversely, the signal from W6 exhibits a clearer correlation than that from W3 and W4 (Fig. 4c), indicating that the former has more significant power. It is noticed that the infrasonic power does not necessarily represent the amount of ash emission. The generation mechanism of infrasound accompanying phreatic eruptions is only partially understood (e.g., Jolly et al. 2016), and we plan to investigate the source process of the infrasonic signals at Iwo-yama in future work.

# Conclusions

We reconstructed the sequence of the multiple-vent activities of the 2018 small phreatic eruption of the Iwo-yama volcano in Japan by conducting an acoustic cross-correlation analysis between two infrasound sensors. We identified infrasound signals from South Crater that were associated with the eruption onset and the vent widening that had been observed by the monitoring camera. We also constrained the timing of the significant eruptive activity at the individual vents in both South Crater and West Crater during the nighttime, which had not been confirmed visually. The results suggest that the intense eruptions with remarkable infrasound delay several hours to the steaming onsets or the vents' appearance. In addition, it is observed that intense infrasound does not necessarily accompany a large amount of ash emission, as is the case with W6. Our results demonstrate a case of the transition processes of phreatic eruptions that form multiple vents. These findings will be useful in constraining the mechanism and assessing eruption hazards.

# Abbreviations

**KVC**: Kirishima Volcanic Complex

**JMA**: Japan Meteorological Agency

**GSI**: Geospatial Information Authority of Japan

## Declarations

# Ethics approval and consent to participate

*Not applicable*

# Consent for publication

*Not applicable*

# Availability of data and materials

The infrasound data are available from the corresponding author on request. The monitoring camera data belong to the Kagoshima Local Meteorological Office of the Japan Meteorological Agency, so please contact them.

# Competing interests

The authors declare that they have no competing interests.

# Funding

This work was supported by the MEXT Earthquake and Volcano Hazards Observation and Research Program, MEXT Integrated Program for Next Generation Volcano Research and Human Resource Development, ERI JURP 2016B03, and JSPS KAKENHI Grant Number JP20J10734.

# Authors' contributions

DM analyzed the data and drafted the manuscript. TM contributed to the data acquisition and maintaining the observation network. MI supported the analysis and theoretical backgrounds. All of the authors contributed to the interpretations and approved the final manuscript.

# Acknowledgements

We thank Dr. Aizawa and Dr. Tajima for their insightful discussions and comments. We thank the Kagoshima Local Meteorological Office, JMA, who provided the monitoring camera data. The aerial photograph used in Fig. 1 was taken from the GSI Tiles of the Geospatial Information Authority of Japan. This work was supported by the MEXT Earthquake and Volcano Hazards Observation and Research

Program, MEXT Integrated Program for Next Generation Volcano Research and Human Resource Development, ERI JURP 2016B03, and JSPS KAKENHI Grant Number JP20J10734.

# References

1. Anderson JF, Johnson JB, Steele AL, Ruiz MC, Brand BD (2018) Diverse Eruptive Activity Revealed by Acoustic and Electromagnetic Observations of the 14 July 2013 Intense Vulcanian Eruption of Tungurahua Volcano, Ecuador. Geophys Res Lett 45(7):2976–2985. https://doi.org/10.1002/2017GL076419
2. Bouche E, Vergniolle S, Staudacher T, Nercessian A, Delmont J-C, Frogneux M, Cartault F, Le Pichon A (2010) The role of large bubbles detected from acoustic measurements on the dynamics of Erta'Ale lava lake (Ethiopia). Earth Planet Sci Lett 295(1–2):37–48. https://doi.org/10.1016/j.epsl.2010.03.020
3. Castaño LM, Ospina CA, Cadena OE, Galvis-Arenas B, Londono JM, Laverde CA, Kaneko T, Ichihara M (2020) Continuous monitoring of the 2015–2018 Nevado del Ruiz activity, Colombia, using satellite infrared images and local infrasound records. Earth Planets Sp 72(1). https://doi.org/10.1186/s40623-020-01197-z
4. Delle Donne D, Ripepe M (2012) High-frame rate thermal imagery of strombolian explosions: Implications for explosive and infrasonic source dynamics. J Geophys Res Solid Earth 117(9). https://doi.org/10.1029/2011JB008987
5. Doke R, Harada M, Mannen K, Itadera K, Takenaka J (2018) InSAR analysis for detecting the route of hydrothermal fluid to the surface during the 2015 phreatic eruption of Hakone Volcano, Japan. Earth Planets Sp 70(1). https://doi.org/10.1186/s40623-018-0834-4
6. Fee D, Garces M, Steffke A (2010) Infrasound from Tungurahua volcano 2006–2008: Strombolian to Plinian eruptive activity. J Volcanol Geotherm Res 193(1–2):67–81. https://doi.org/10.1016/j.jvolgeores.2010.03.006
7. Fee D, Matoza RS (2013) An overview of volcano infrasound: From Hawaiian to Plinian, local to global. J Volcanol Geotherm Res 249:123–139. https://doi.org/10.1016/j.jvolgeores.2012.09.002
8. Garcés M, Harris A, Hetzer C, Johnson J, Rowland S, Marchetti E, Okubo P (2003) Infrasonic tremor observed at Kīlauea Volcano, Hawai'i. Geophys Res Lett 30(20). https://doi.org/10.1029/2003gl018038
9. Ichihara M, Takeo M, Yokoo A, Oikawa J, Ohminato T (2012) Monitoring volcanic activity using correlation patterns between infrasound and ground motion. Geophys Res Lett 39(4). https://doi.org/10.1029/2011GL050542
10. Ishii K, Yokoo A, Kagiyama T, Ohkura T, Yoshikawa S, Inoue H (2019) Gas flow dynamics in the conduit of Strombolian explosions inferred from seismo-acoustic observations at Aso volcano, Japan. Earth Planets Sp 71(1). https://doi.org/10.1186/s40623-019-0992-z

11. Johnson JB (2003) Generation and propagation of infrasonic airwaves from volcanic explosions. J Volcanol Geotherm Res 121(1–2):1–14. https://doi.org/10.1016/S0377-0273(02)00408-0
12. Johnson JB, Ripepe M (2011) Volcano infrasound: A review. J Volcanol Geotherm Res 206(3–4):61–69. https://doi.org/10.1016/j.jvolgeores.2011.06.006
13. Jolly A, Kennedy B, Edwards M, Jousset P, Scheu B (2016) Infrasound tremor from bubble burst eruptions in the viscous shallow crater lake of White Island, New Zealand, and its implications for interpreting volcanic source processes. J Volcanol Geotherm Res 327:585–603. https://doi.org/10.1016/j.jvolgeores.2016.08.010
14. Matoza RS, Arciniega-Ceballos A, Sanderson RW, Mendo-Pérez G, Rosado-Fuentes A, Chouet BA (2019) High-Broadband Seismoacoustic Signature of Vulcanian Explosions at Popocatépetl Volcano, Mexico. Geophys Res Lett 46(1):148–157. https://doi.org/10.1029/2018GL080802
15. Matoza RS, Fee D, Garcés MA, Seiner JM, Ramón PA, Hedlin MAH (2009) Infrasonic jet noise from volcanic eruptions. Geophys Res Lett 36(8). https://doi.org/10.1029/2008GL036486
16. McKee K, Fee D, Haney M, Matoza RS, Lyons J (2018) Infrasound Signal Detection and Back Azimuth Estimation Using Ground-Coupled Airwaves on a Seismo-Acoustic Sensor Pair. J Geophys Res Solid Earth 123(8):6826–6844. https://doi.org/10.1029/2017JB015132
17. Perttu A, Taisne B, Angelis S, De, Assink JD, Tailpied D, Williams RA (2020) Estimates of plume height from infrasound for regional volcano monitoring. J Volcanol Geotherm Res 402(15). https://doi.org/10.1016/j.jvolgeores.2020.106997
18. Ripepe M, De Angelis S, Lacanna G, Voight B (2010) Observation of infrasonic and gravity waves at Soufrière Hills Volcano, Montserrat. Geophys Res Lett 37(8). https://doi.org/10.1029/2010GL042557
19. Ripepe M, Marchetti E (2002) Array tracking of infrasonic sources at Stromboli volcano. Geophys Res Lett 29(22):33-1-33–4. https://doi.org/10.1029/2002gl015452
20. Tajima Y, Nakada S, Maeno F, Huruzono T, Takahashi M, Inamura A, Matsushima T, Nagai M, Funasaki J (2020) Shallow Magmatic Hydrothermal Eruption in April 2018 on Ebinokogen Ioyama Volcano in Kirishima Volcano Group. Kyushu Japan Geosciences 10(5):183. https://doi.org/10.3390/geosciences10050183
21. Tajima Y, Nakada S, Nagai M, Maeno F, Watanabe A (2019) Small eruption at the Ebinokogen Ioyama volcano of the Kirishima Volcano Group in April 2018. Bull Volcanol Soc Japan 64(2):147–151. https://doi.org/10.18940/kazan.64.2_147
22. Tsukamoto K, Aizawa K, Chiba K, Kanda W, Uyeshima M, Koyama T, Utsugi M, Seki K, Kishita T (2018) Three-Dimensional Resistivity Structure of Iwo-Yama Volcano, Kirishima Volcanic Complex, Japan: Relationship to Shallow Seismicity, Surface Uplift, and a Small Phreatic Eruption. Geophys Res Lett 45(23):12,821 –821 12,828. https://doi.org/10.1029/2018GL080202
23. Vergniolle S, Brandeis G (1996) Strombolian explosions 1. A large bubble breaking at the surface of a lava column as a source of sound. J Geophys Res B Solid Earth 101(9):20433–20447. https://doi.org/10.1029/96jb01178

24. Walsh B, Procter J, Lokmer I, Thun J, Hurst T, Christenson B, Jolly A (2019) Geophysical examination of the 27 April 2016 Whakaari/White Island, New Zealand, eruption and its implications for vent physiognomies and eruptive dynamics. Earth Planets Sp 71(1). https://doi.org/10.1186/s40623-019-1003-0
25. Yamada T, Aoyama H, Nishimura T, Iguchi M, Hendrasto M (2017) Volcanic eruption volume flux estimations from very long period infrasound signals. Geophys Res Lett 44(1):143–151. https://doi.org/10.1002/2016GL071047
26. Yamada T, Aoyama H, Ueda H (2018) Relationship between infrasound-derived and buoyancy-derived eruption plume volume estimates. Bull Volcanol 80(9). https://doi.org/10.1007/s00445-018-1244-y
27. Yamakawa K, Ichihara M, Ishii K, Aoyama H, Nishimura T, Ripepe M (2018) Azimuth Estimations From a Small Aperture Infrasonic Array: Test Observations at Stromboli Volcano, Italy. Geophys Res Lett 45(17):8931–8938. https://doi.org/10.1029/2018GL078851
28. Yamasato H (1997) Quantitative analysis of pyroclastic flows using infrasonic and seismic data at Unzen volcano, Japan. J Phys Earth 45(6):397–416. https://doi.org/10.4294/jpe1952.45.397
29. Yokoo A, Tameguri T, Iguchi M (2009) Swelling of a lava plug associated with a Vulcanian eruption at Sakurajima Volcano, Japan, as revealed by infrasound record: Case study of the eruption on January 2, 2007. Bull Volcanol 71(6):619–630. https://doi.org/10.1007/s00445-008-0247-5
30. Yukutake Y, Honda R, Harada M, Doke R, Saito T, Ueno T, Sakai S, Morita Y (2017) Analyzing the continuous volcanic tremors detected during the 2015 phreatic eruption of the Hakone volcano. Earth Planets Sp 69(1):164. https://doi.org/10.1186/s40623-017-0751-y
31. Yukutake Y, Ichihara M, Honda R (2018) Infrasonic wave accompanying a crack opening during the 2015 Hakone eruption. Earth Planets Sp 70(1). https://doi.org/10.1186/s40623-018-0820-x

# Figures

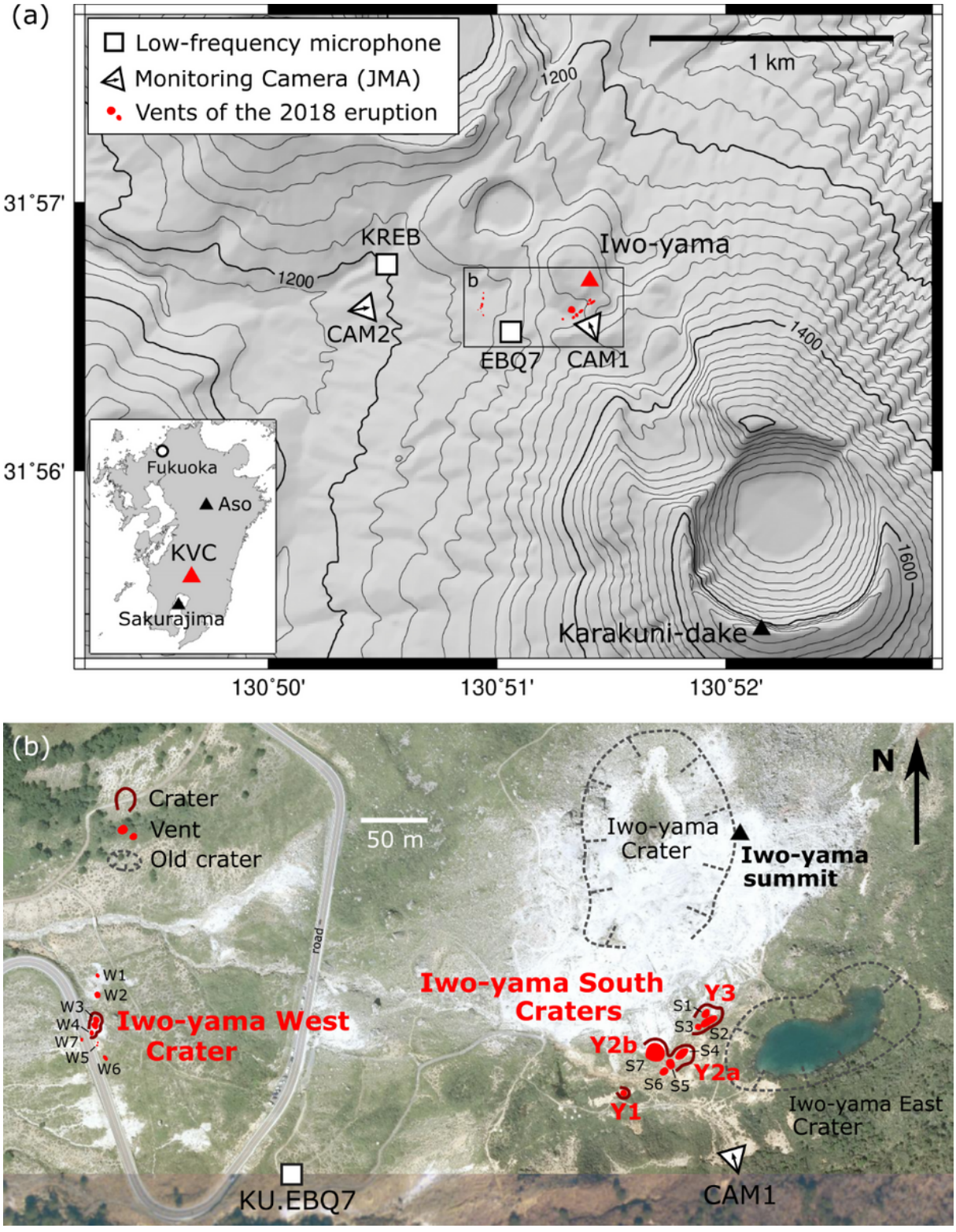


## Figure 1

Observation sites and crater locations. (a) Iwo-yama volcano (summit is indicated by the red triangle) and the locations of the observation sites. The contour interval is 20 m. The small red circles are the vents of the 2018 small phreatic eruption. The region surrounded by the rectangle is enlarged in (b). Map insert shows the location of Kirishima Volcanic Complex (KVC) on Kyushu Island, southwest of Japan. (b) Craters and vents of the eruption. There are two main craters, Iwo-yama South Craters and Iwo-yama

West Crater. The South Crater was composed of four vents; Y1, Y2a, Y2b, and Y3. Y1 vent appeared on April 7, 12 days before the eruption. We excluded Y1 from the discussion because it did not participate in the eruption. Locations of the craters and vents were cited from Tajima et al. (2020). The photograph was taken from GSI Tiles, of the Geospatial Information Authority of Japan.

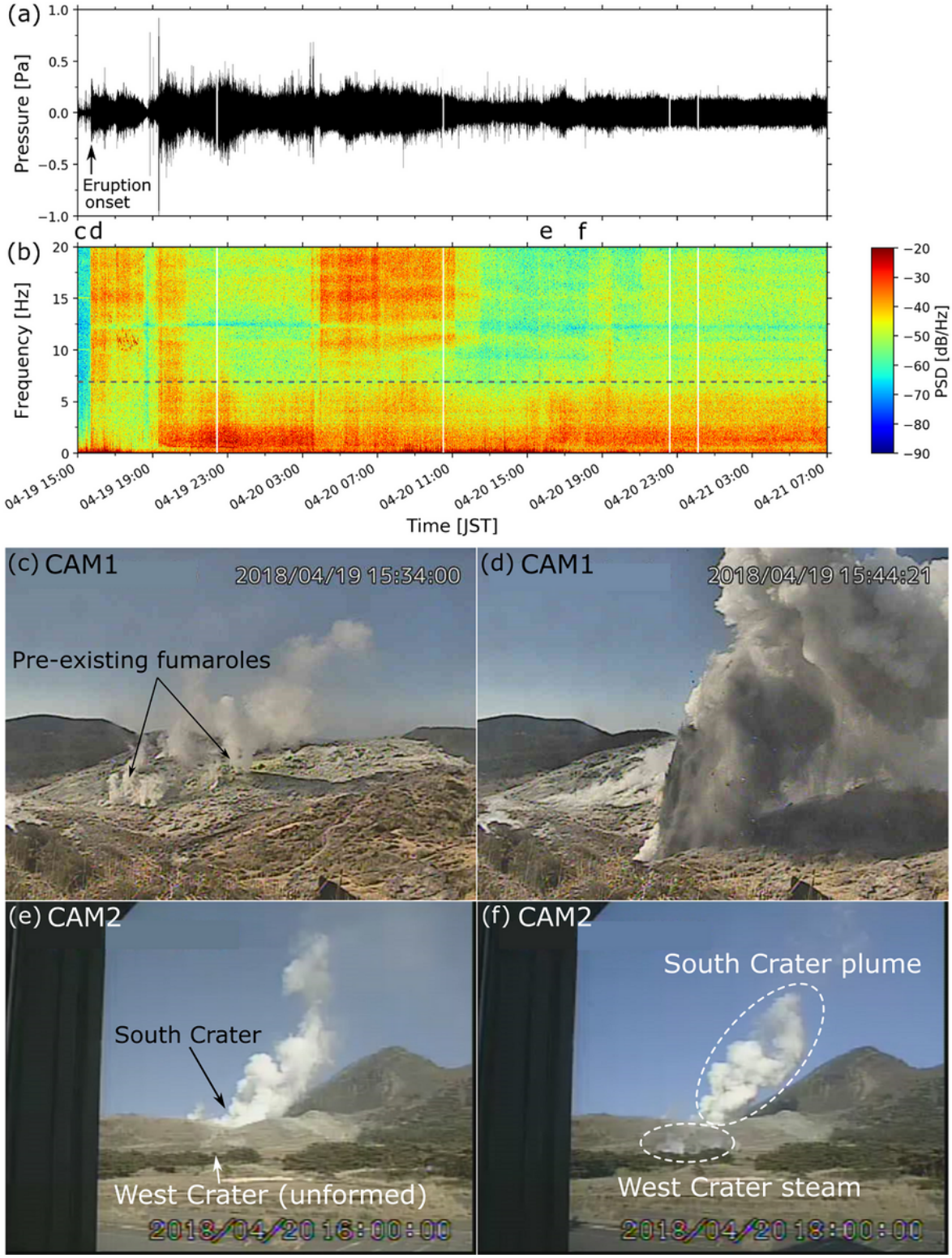


**Figure 2**

Waveform and spectrogram of infrasound recorded by MC2 and the snapshots that captured surface phenomena associated with the eruption by CAM1 and CAM2. (a) Infrasound waveform filtered 0.3–20 Hz. The vertical white lines represent data-missing periods due to equipment problems. (b) Spectrogram of the nonfiltered infrasonic signal calculated using 10.24 s sliding windows with 50% overlaps. We found infrasonic powers in two frequency bands separated at 7 Hz (gray dashed line). The middle panels show snapshots of South Craters taken by CAM1 just prior to the eruption (c) and at the onset of the eruption (d). The bottom panels are snapshots taken by CAM2 that show West Crater before the eruption (e) and emitting faint steam (f).

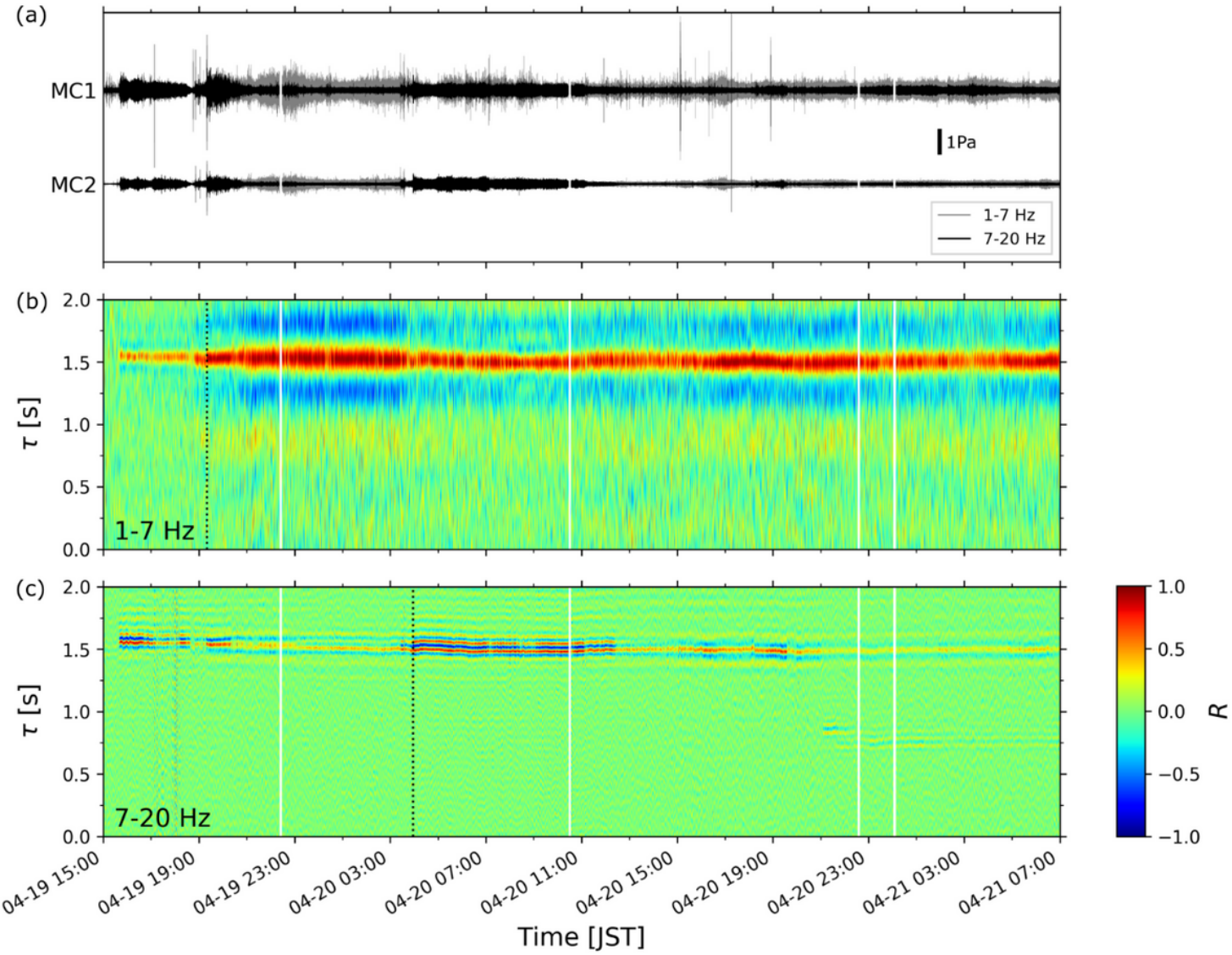


## Figure 3

Cross-correlation analysis between MC1 and MC2. The vertical white lines represent data-missing periods. (a) Waveforms filtered 1–7 Hz (gray lines) and 7–20 Hz (black lines) recorded by MC1 and MC2. (b) The t-τ plot of the cross-correlation coefficient in the frequency range of 1–7 Hz. The signal starts with the eruption onset at 15:39:45 on April 19, and the correlation values increase from 19:19:40 on April 19

(black dotted line). (c) The cross-correlation coefficient in the frequency range of 7–20 Hz. The correlation peaks appear with the eruption onset and re-intensify after around 3:57 on April 20 (black dotted line).

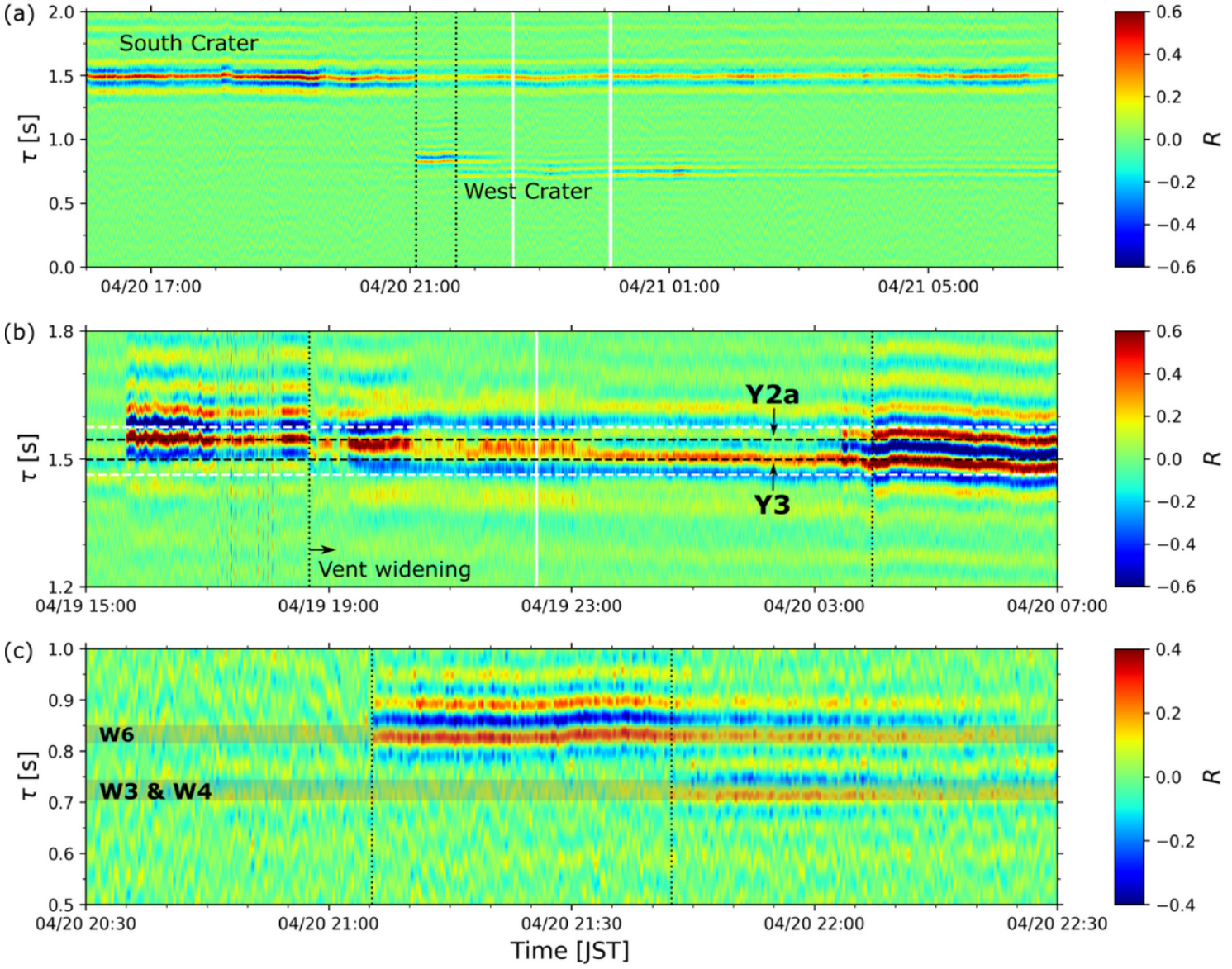


## Figure 4

Stacked cross-correlation coefficients for the higher-frequency band. (a) The t-τ plot of the stacked cross-correlation coefficients in the frequency range of 7–20 Hz from 16:00 on April 20 to 7:00 on April 21. The vertical white lines represent data-missing periods. (b) The plot focusing on South Crater signals from 15:00 on April 19 to 7:00 on April 20. The expected lag time ranges of South Crater (1.46–1.58 s) are bounded by the horizontal white dashed lines. The horizontal black dashed lines are τ=1.55 s and 1.50 s, corresponding to Y2a and Y3, respectively. The vertical dotted lines mark times of the vent widening onset (18:40:51 on April 19) and re-increase of the high-frequency signal power (3:57:00, on April 20). (c) Enlarged view of the t-τ plot from 20:30 to 22:30 on April 20. Gray shaded regions indicate the expected lag times of the vents W3–W4 and W6. The clear signals appear at 21:05:20 from W6 and at 21:42:20 from W3–W4 (vertical dotted lines).

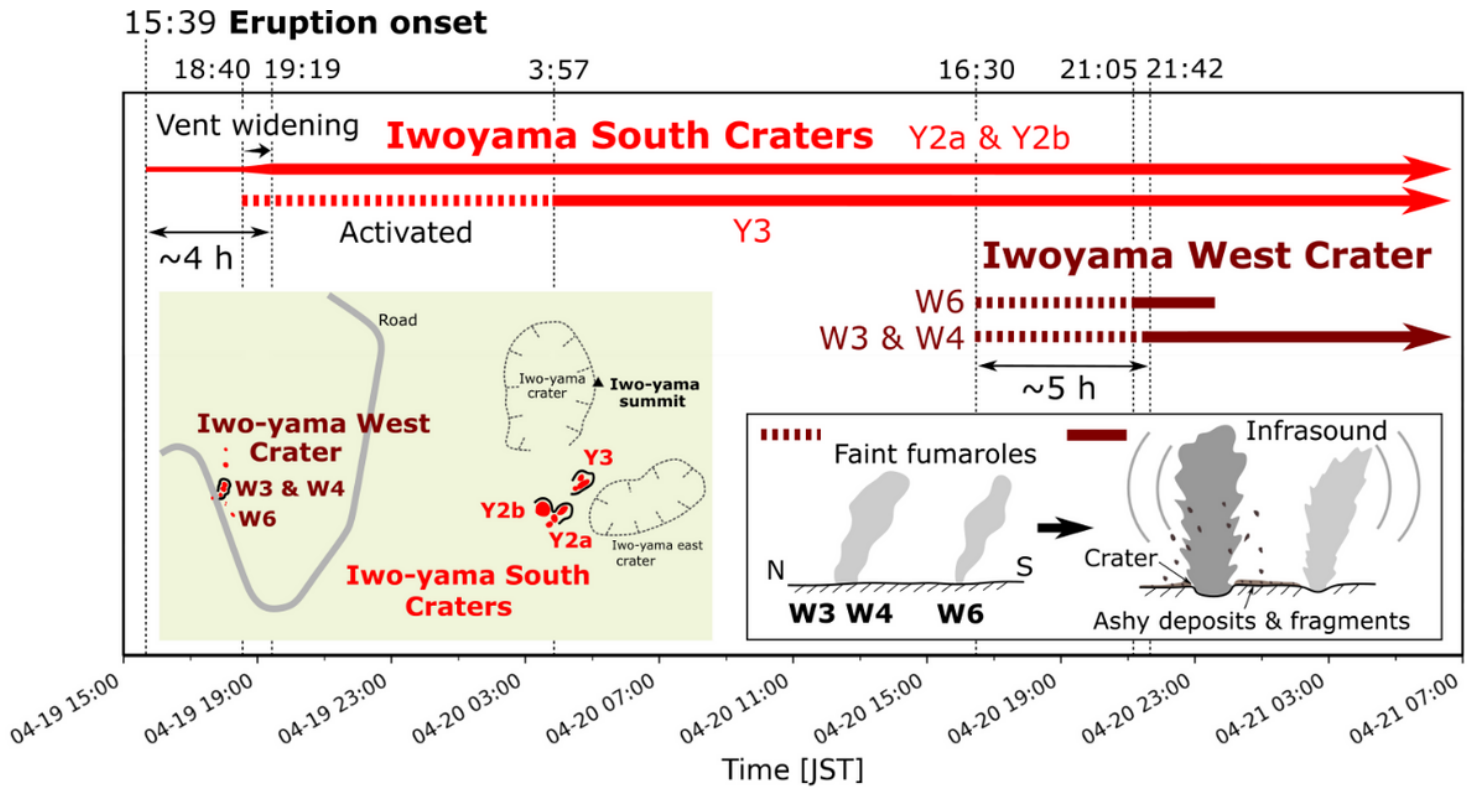


**Figure 5**

Summary of the reconstructed sequence of the 2018 small phreatic eruption of Iwo-yama volcano. The eruption began at 15:39 on April 19 at Y2a in the South Crater area. The Y2a vent widened from 18:40, and then the eruption intensified from 19:19. Simultaneously with the vent widening, Y3 was activated and then became the main source of high frequency infrasonic signals after 3:57 on April 20. Weak fumaroles appeared in the West Crater area around 16:30 on April 20. An eruption or gas emission started from 21:05 at W6. A small eruption emitting ash and ejecta occurred at 21:42 at W3–W4, resulting in the formation of a crater.

# Supplementary Files

This is a list of supplementary files associated with this preprint. Click to download.

- AdditionalFile1.pdf
- AdditionalFile2.pdf
- AdditionalFile3.pdf
- GraphicalAbstract.png